

# PhysDepth: Plug-and-Play Physical Refinement for Monocular Depth Estimation in Challenging Environments

Kebin Peng<sup>1</sup> Haotang Li<sup>2</sup> Zhenyu Qi<sup>2</sup> Huashan Chen<sup>3,4</sup>  
Zi Wang<sup>5</sup> Wei Zhang<sup>5</sup> Sen He<sup>2</sup> Huanrui Yang<sup>2</sup> Qing Guo<sup>6</sup>

<sup>1</sup> Department of Computer Science, East Carolina University, Greenville, NC, USA

<sup>2</sup> Department of Electrical and Computer Engineering, The University of Arizona, Tucson, AZ, USA

<sup>3</sup> Institute of Information Engineering, Chinese Academy of Sciences, Beijing, China

<sup>4</sup> School of Cyber Security, University of Chinese Academy of Sciences, Beijing, China

<sup>5</sup> School of Computer and Cyber Sciences, Augusta University, Augusta, GA, USA

<sup>6</sup> VCIP, CS, Nankai University, China

## Abstract

State-of-the-art monocular depth estimation (MDE) models often struggle in challenging environments, primarily because they overlook robust physical information. To demonstrate this, we first conduct an empirical study by computing the covariance between a model’s prediction error and atmospheric attenuation. We find that the error of existing SOTAs increases with atmospheric attenuation. Based on this finding, we propose PhysDepth, a plug-and-play framework that solves this fragility by infusing physical priors into modern SOTA backbones. PhysDepth incorporates two key components: a Physical Prior Module (PPM) that leverages Rayleigh Scattering theory to extract robust features from the high-SNR red channel, and a physics-derived Red Channel Attenuation Loss (RCA) that enforces model to learn the Beer-Lambert law. Extensive evaluations demonstrate that PhysDepth achieves SOTA accuracy in challenging conditions.

## 1. Introduction

Monocular depth estimation (MDE) is a fundamental task for autonomous driving [31, 51] and robotics [7, 61]. While recent self-supervised methods have advanced significantly, their performance remains inherently limited by a primarily data-driven paradigm [12, 15, 24, 36, 41, 45–47, 49, 60]. This reliance forces models to learn brittle, non-physical heuristics (e.g., ‘finer texture: closer’ or ‘brighter lights: closer’) rather than robust physical principles. These spurious correlations often struggle in challenging environments, resulting in suboptimal results.

The fundamental problem is that existing SOTA methods

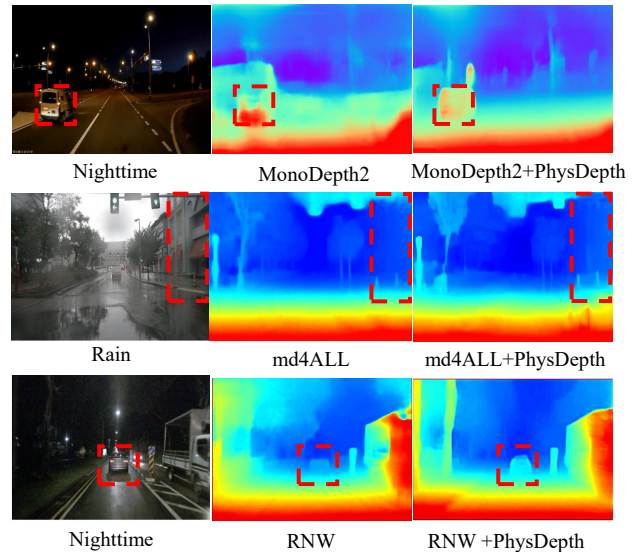


Figure 1. **Plug-and-Play of the PhysDepth.** we show that adding PhysDepth to a baselines like MonoDepth2 [15], md4ALL[12], and RNW [49] effectively corrects common failure modes.

overlook robust physical information.

Motivated by this, we develop PhysDepth, a novel self-supervised MDE framework that infuses physical priors, Rayleigh Scattering theory and Beer-Lambert law, into modern SOTA backbones (e.g., ViT and ConvNeXt). Specifically, PhysDepth enhances base MDE model with two key components: a *Physical Prior Module (PPM)* and a *Red Channel Attenuation Loss (RCA)*. The PPM, guided by Rayleigh Scattering, extracts robust features from the high-SNR red channel. The RCA loss, derived from the Beer-Lambert law, enforces a physically-consistent relationship between this attenuation signal and the final depth.

As illustrated in Figure 1, SOTA MDE models, includ-

ing MonoDepth2 [15], md4ALL[12], and RNW [49] fail in challenging environments, producing hazardous artifacts from real-world conditions like road reflections and glare.

By plugging in PhysDepth, enhanced MDE models can produce visually clean and accurate results. Furthermore, our quantitative analysis in Table 5 shows that when we plug PhysDepth into existing SOTA backbones, their performance has been significantly improved.

In summary, the key contributions of this paper include:

- We find that existing SOTA MDE models overlook physical information. To prove this, we conduct an empirical study that measures the correlation between atmospheric attenuation and the model’s error metric.
- We propose PhysDepth, a novel plug-and-play framework that addresses this fragility by explicitly integrating physical priors (Rayleigh Scattering and Beer-Lambert law) into diverse modern backbones.
- We introduce a Physical Prior Module (PPM) and a physics-derived Red Channel Attenuation Loss (RCA), which together form a portable plugin for different MDE architectures.
- Extensive evaluations demonstrate that PhysDepth achieves SOTA performance in challenging conditions, and prove the generality of our plug-and-play approach.

## 2. Related Work

Depth estimation under challenging conditions (e.g., rain or night) has attracted increased attention recently. Some SOTA methods focus on feature representation and regularizers. For example, Zhang et al. [57] leverages CoMoGAN to transform daytime images into challenging scenes, thereby circumventing the need for a separate nighttime dataset. Yan et al. [54] also use synthetic adverse data to train their model. Zhang et al [58] use CLIP and DINO under contrastive language guidance for dark images. Chung et al. [4] proposed a test-time adaptation for challenging condition depth estimation. DeFeat-Net [41] uses a cross-domain dense feature representation. RNW [49] uses image enhancement and a GAN-based regularizer. Cong et al. [5] introduce a structure-regularized framework cropped multi-scale consistency loss for low visibility and illumination conditions. Meanwhile, other SOTA methods focus on domain adaptation networks. ADIDS [24] uses two networks for day-time and nighttime images. Vankadari et al. [45] and ITDFA [59] both adapted a domain adaptation network trained on daytime images to function in dark environments. Gasperini et al. [12] also convert challenging environment images to daytime conditions using a translation model. WSGD [46] adds denoising into domain adaptation network. Hou et al. [19] introduce an illumination compensation PoseNet for lighting adaptation, and a cross-layer adaptive fusion module to enhance feature complementarity. Sharma et al. [39] developed a translation network to

create nighttime stereo images from daytime versions, then trained on a stereo network. Also, some SOTA methods use additional information. Lu et al. [26] combined thermal and RGB data to enhance the accuracy of nighttime depth estimation. R4dyn [11] uses radar at nighttime.

## 3. PhysDepth: Motivation & Method

### 3.1. Empirical Study, Motivation, and Base Model

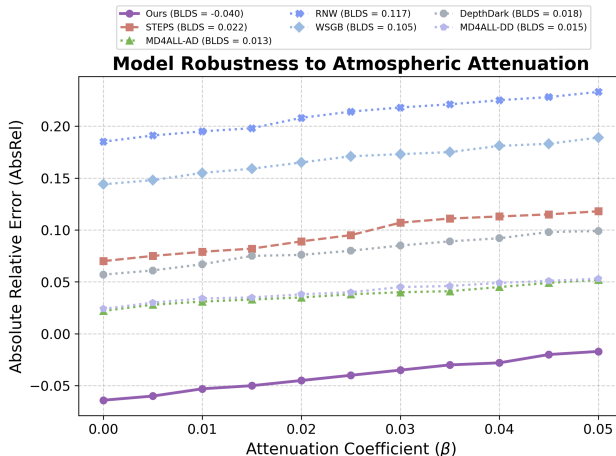


Figure 2. **Quantitative Analysis of Robustness to Atmospheric Attenuation.** Quantitative comparison of model robustness against increasing atmospheric attenuation ( $\beta$ ). Our method (purple line) achieves the lowest Absolute Relative Error (AbsRel) and the flattest performance curve.

We argue that existing SOTA methods overlook robust physical information. To prove this, we conduct an empirical study that measures the covariance  $Cov$  between a model’s error metric and a controlled, physically-plausible injection of atmosphere attenuation  $\beta$  [17].

This study uses a test set containing challenging condition images  $I$  and corresponding ground-truth depth maps  $D_{gt}$ . We generate a sequence of perturbed images by applying the volumetric scattering model [9, 17, 29, 30, 42] in Equation 1 :

$$I'(x) = J(x) \cdot t(x) + A \cdot (1 - t(x)) \quad (1)$$

We use algorithm 1 in supplemental material to compute  $Cov$ , and we define the parameters as follows:

- Scene Radiance  $J(x)$ : We approximate the clear-night radiance using the input image:  $J(x) \approx I(x)$ .
- Airlight  $A$ : This term represents ambient light scattered into the camera path. Critically, for a nocturnal scene, we fix a neutral, dark airlight, representative of ambient light pollution or environmental glow, such as  $A = [0.1, 0.1, 0.1]$  in RGB space. This correctly simulates the "black-point" elevation observed in low-visibility conditions (e.g., night).

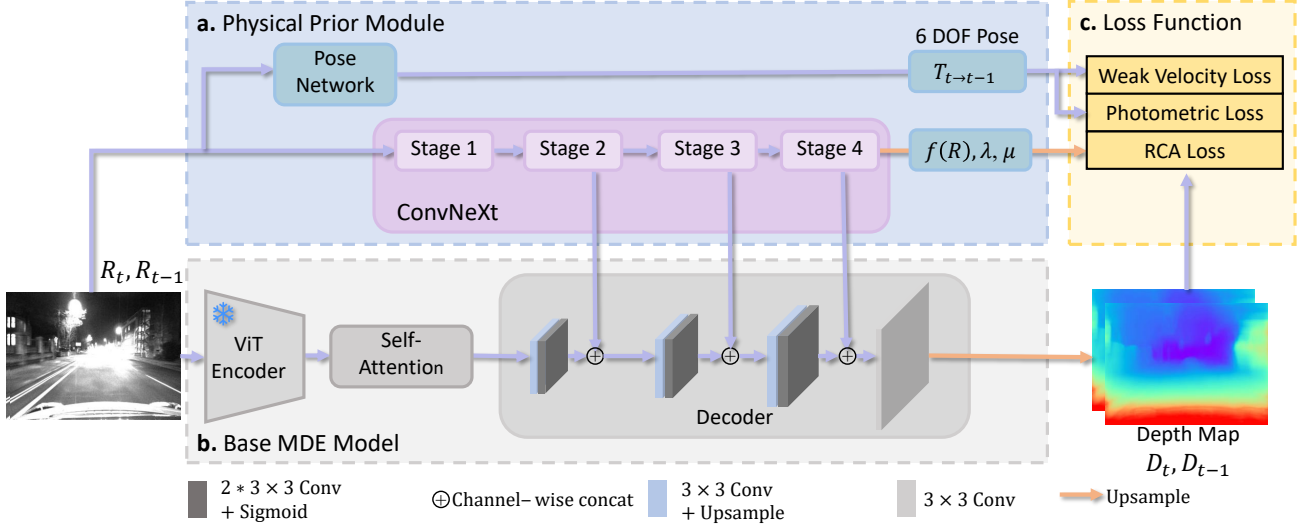


Figure 3. **PhysDepth Architecture** contains three parts: (a) The Physical Prior Module (PPM), which uses a ConvNeXt backbone to extract hierarchical features from the red channels ( $R_t, R_{t-1}$ ). (b) The Base MDE Model, which uses a ViT Encoder and a Decoder to predict depth from the full image. The PPM’s features are fused into the Base Decoder at multiple scales. (c) The Loss Function, which includes our RCA Loss that supervises the PPM.

- Transmission  $t(x)$ : The transmission is governed by the Beer-Lambert law,  $t(x) = \exp(-\beta \cdot D_{gt}(x))$ , where  $\beta$  is the extinction coefficient that controls the density of the attenuation (e.g., light fog or mist).
- Perturbation Vector  $\mathbf{B}$ : We define a vector of  $N$  extinction coefficients,  $\mathbf{B} = [\beta_0, \beta_1, \dots, \beta_N]$ . A typical range is  $\beta_i \in [0.0, 0.05]$ , where  $\beta_0 = 0.0$  represents the original, clear-night image.
- Error function Error: We use *AbsRel* here, a "lower-is-better" metric.

**Interpretation of the covariance.** As shown in Figure 2, Our PhysDepth (purple solid line) achieves the lowest AbsRel error across the entire range of attenuation coefficients, consistently and significantly outperforming all competing models. As  $\beta$  increases, the error of all models rises. However, PhysDepth exhibits the flattest performance curve, indicating that its performance degrades the least as conditions worsen. This superior stability is also quantified by the *Cov* score shown in the legend; our method achieves the best (lowest) score of -0.040, while all other methods have positive (worse) scores, confirming its exceptional robustness to challenging environments. Also, PhysDepth’s  $Cov < 0$  means that it has successfully learned the physical priors, treating attenuation as a valid, independent signal for depth. SOTAs such as STEPS [60], DepthDark [56], md4ALL-AD [12], md4ALL-DD [12], their  $Cov \approx 0.0$  (No Correlation) means each model’s performance is decoupled from attenuation, indicating it *only rely on other cues*, such as semantic context or geometry. For other methods like WSGB [46] and RNW [49], their  $Cov > 0$  (Positive Correlation) indicates that each model treats attenuation as noise that occludes its primary cues. This empirical study

motivates us to design PhysDepth based on robust physical information.

Figure 3 illustrates the design of PhysDepth. We select a modern Transformer-based architecture as the encoder in our primary Base MDE Models (Figure 3 - b). We also follow Piccinelli et al. [35] to employ both ConvNeXt-T [25] and MiDaS [37] to serve as the encoder in the base model.

### 3.2. Physical Prior Module

Rayleigh Scattering theory depicts the relationship between wavelength and the amount of scattered light (Equation 2, where  $I_s$  is the intensity of scattered light, and  $\lambda$  is the wavelength). Specifically, red light, due to its longer wavelength, is less likely to be scattered than blue and green light. Thus, *red channel image is more likely to preserve details for MDE, especially under challenging lighting conditions.*

$$I_s \propto \frac{1}{\lambda^4} \quad (2)$$

We start by conducting experiments to verify the relationships between image channels and the accuracy of MDE results. Particularly, RGB images from RobotCar-Night dataset [27] are replaced by their single-channel images and two-channel images for comparison, respectively. We use the base MDE model, Pose Network, and Photometric Loss in Figure 3 as a baseline. Table 1 shows that single-channel image settings outperform their two-channel counterparts, surpassing RGB image settings. Notably, the red channel setting (Baseline+R) yields the best results.

The red channel’s superior performance attributes to a two-fold physical advantage: **1) Rayleigh Scattering**: light is scattered by the atmospheric medium itself, even in clear

Table 1. **Using Different Channel Images from RobotCar-Night Dataset [27]:** R means Red Channel, so do B (Blue Channel) and G (Green Channel), RGB. The best results are in **bold**. Base MDE model uses ViT-B/.

| Methods           | Abs Rel        | Sq Rel       | RMSE         | RMSE log     |
|-------------------|----------------|--------------|--------------|--------------|
|                   | lower's better |              |              |              |
| Baseline+RGB      | 0.690          | 8.215        | 7.105        | 0.473        |
| Baseline+B+R      | 0.673          | 8.211        | 7.105        | 0.473        |
| Baseline+G+R      | 0.675          | 8.212        | 7.103        | 0.471        |
| Baseline+B+G      | 0.671          | 8.210        | 7.104        | 0.469        |
| Baseline+B        | 0.668          | 8.209        | 7.098        | 0.465        |
| Baseline+G        | 0.667          | 8.209        | 7.098        | 0.463        |
| <b>Baseline+R</b> | <b>0.665</b>   | <b>8.206</b> | <b>7.097</b> | <b>0.461</b> |

air. This law states that the shorter-wavelength blue and green channels are scattered more than the red channel, degrading their signal integrity over distance. **2) Signal-to-Noise Ratio (SNR):** This fundamental scattering advantage is compounded by the realities of challenging-condition illumination. Artificial lighting (e.g., brake lights, street-lights) is mainly red/yellow. As a result, the sensor’s red channel receives a stronger and cleaner signal, while the blue and green channels are more likely to capture sensor noise. Furthermore, combining multiple channels can introduce additional noise [18], leading to inaccurate MDE results. Thus, we use **red channel images** for PhysDepth.

To take full advantage of red channel images, we propose PPM (Figure 3 - a), which aims to enable backbone (e.g., ViT-B/32) and pose estimation network to *explicitly* and *comprehensively* learn the relationships between red channel values and depth values.

To implement PPM, we employ a modern hierarchical backbone, ConvNeXt [25], to extract image features and establish the correlation between red channel values and depth values (Figure 3 - a). To enhance the robustness of the Base MDE Model, we inject the physical features from the PPM at multiple scales. The intermediate feature maps from the ConvNeXt encoder stages (Stage 2, Stage 3, Stage 4) are fused with the feature maps of the Base MDE Decoder at corresponding resolutions via channel-wise concatenation.

The output of PPM is the predicted depth map from red channel image. It also serves as part of the inputs of RCA loss (See Section 3.3). Simultaneously, the predicted depth map from the decoder serves as the other part of RCA loss input. To match the dimensions of the predicted depth map, the last layer of PPM’s output requires an up-sampling layer. One noteworthy difference between our PPM and a standard ConvNeXt encoder is that, while they both output the same dimension for depth estimation, PPM, in addition, outputs additional two channels for estimating  $\mu$  and  $\lambda$  for RCA loss in Equation 6.

### 3.3. Red Channel Attenuation Loss (RCA loss)

To guide the training processes of PPM, we introduce RCA loss (Figure 3 - c). RCA loss is based on Beer-Lambert law (Equation 3) and Rayleigh scattering theory (Equation 2).

$$I = I_0 e^{-\mu d_R} \quad (3)$$

Specifically, in our model, we consider Equation 3 for each pixel, where  $I_0$  denotes the intensity of the luminous point.  $I$  denotes the light intensity after attenuation.  $\mu$  is a constant and  $d$  is depth value.  $e^{-\mu d_R}$  is the attenuation item. Also, we discuss the different items in Section 11 in Supplementary Material.

Equation 3 suggests the possibility of deriving the depth value, denoted as  $d_R$  from the information contained in  $I$  and  $I_0$ . This insight motivates us to employ it as a loss function during the training of PPM. To facilitate this, we rephrase Equation 3 to Equation 4 as:

$$d_R = -\frac{1}{\mu} \ln I + \frac{\ln I_0}{\mu} \quad (4)$$

We then use gradient Spherical Gaussian (SG) [22, 48, 52] to model  $I_0$  in Equation 5, where  $\lambda \in \mathbb{R}$  is a learnable parameter. It is because the naive application of the Beer-Lambert law would require solving for the per-pixel intrinsic brightness  $I_0$ , which is ill-posed from a single image. We instead simplify this term by modeling its contribution as a single, globally learnable parameter  $\lambda$ . We are therefore not claiming to model the true  $I_0$  of every pixel. Rather, the term  $\frac{1}{\mu}(g\lambda - 1)$  functions as a learned scalar bias in the regression. This simplification makes the problem tractable and prevents the model from learning a trivial identity by encoding depth in the  $I_0$  term.

In our experiments, we empirically set  $g = 1.3938$  for the best accuracy.

$$I_0 = e^{g\lambda - 1} \quad (5)$$

Additionally, as discussed in Section 3.2, the phenomenon of Rayleigh scattering theory drives our decision to focus on the attenuation of red channel in our architecture. Thus, we replace the RGB image  $I$  with red channel image  $R$ , and  $f(R)$  represents the feature from the last layer of PPM. Mathematically, our goal is for the final layer to learn an identity map ping,  $f(R) = R$ . And we apply the law to  $f(R)$ , the output of the PPM, rather than the raw pixel intensity  $R$ . This is a principled design choice, as raw pixel values are a poor proxy for true physical radiance. The  $R$  value is corrupted by non-linearities from the camera’s Image Signal Processor (e.g., gamma correction, tonemapping) and sensor noise. The PPM ( $f(R)$ ) is trained to learn a linearized, denoised representation of the scene’s radiance. Therefore,  $f(R)$  serves as a more suitable and

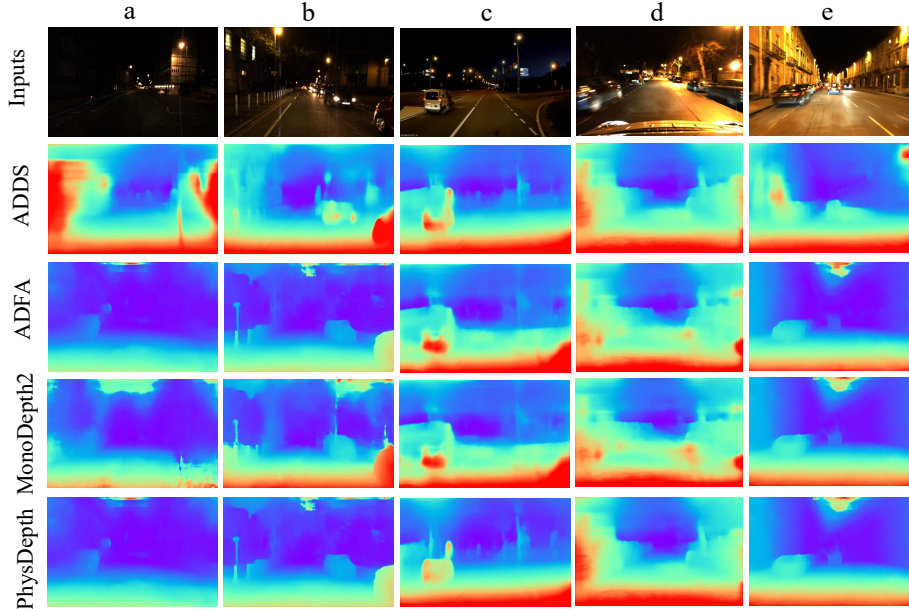


Figure 4. **Qualitative Results - RobotCar-Night:** Depth estimated on five different test images (row: Inputs) using our model (row: PhysDepth) and three SOTA (remaining rows) for comparison.

physically valid input for the Beer-Lambert law than  $R$  itself Table 16 in supplemental material. Taking gradient SG and  $f(R)$  into account, we can now reformulate Equation 4 to Equation 6 as follow:

$$d_R = -\frac{1}{\mu} \ln f(R) + \frac{1}{\mu} (g\lambda - 1) \quad (6)$$

Then we apply Equation 6 to train PPM. Specifically, when we know  $d_R$ , we use  $\mathcal{L}_2$  to denote L2 loss and compute  $\mathcal{L}_2$  between  $d_R$  and  $d_{ES}$ .  $d_{ES}$  is the estimated depth map from Base MDE decoder. *Because the attenuation has a functional relation  $\ln f(R)$  with depth value  $d_R$ , it can be used to supervise the training of PPM*, which is the mathematical foundation of our design choice.

#### Total Training Loss Function,

RCA loss serves as a self-supervised signal to guide the training processes of PPM. Besides RCA loss, we also train our model with another supervisory signal: photometric reconstruction loss function  $\mathcal{L}_p$  from SfMLearner [62]. It requires four inputs as Figure 3 shows: Image  $R_t, R_{t-1}$ , Transformation  $T_{t \rightarrow t-1}$ , predicted depth map  $D_t$ , and camera intrinsics matrix  $K$ . We add the weak velocity supervision  $\mathcal{L}_v$  [16] to address scale ambiguity and ensure consistent predictions of photometric reconstruction [12]. Also following [12, 15], we consider partial occlusions via the minimum reprojection error  $\mathcal{L}_p$ , and we ignore static pixels. Another loss  $\mathcal{L}_s$  is used to promote smoothness and preserves edges [14] The total loss function is  $\mathcal{L} = \mathcal{L}_p + \mathcal{L}_2 + \mathcal{L}_v + \mathcal{L}_s$ .

Table 2. **Quantitative Results - RobotCar-Night [27]:** We scale depth up to 50 meters as same as [12, 46]. The best results are in **bold** for each metric. The results presented here are without post-processing. AD and DD mean different training strategies for md4All.

| Methods             | Abs Rel        | RMSE         | $\delta < 1.25$ |
|---------------------|----------------|--------------|-----------------|
|                     | lower's better |              | higher's better |
| MonoDepth2 [15]     | 0.453          | 11.420       | 0.700           |
| DeFeat-Net [41]     | 0.334          | 8.606        | 0.586           |
| ADDS [24]           | 0.287          | 7.985        | 0.490           |
| DepthSegNet24 [43]  | 0.195          | 5.936        | 0.734           |
| ADFA [45]           | 0.231          | 8.800        | 0.620           |
| RNW [49]            | 0.185          | 6.549        | 0.733           |
| WSGD [46]           | 0.174          | 6.302        | 0.754           |
| STEPS [60]          | 0.170          | 6.797        | 0.758           |
| DepthDark [56]      | 0.157          | 4.284        | 0.760           |
| md4All-AD [12]      | 0.124          | 3.612        | 0.858           |
| md4All-DD [12]      | 0.122          | 3.604        | 0.849           |
| Syn2Real-Depth [55] | 0.110          | 3.455        | 0.862           |
| <b>PhysDepth</b>    | <b>0.109</b>   | <b>3.450</b> | <b>0.863</b>    |

## 4. Experiments

**Implementation Details:** Our model is built using PyTorch [33]. We train our model with a batch size of 4, Adam optimizer [21] is used with  $\beta_1 = 0.9$  and  $\beta_2 = 0.999$ , we set the learning rate to 0.0002. Meanwhile, we follow Zhou et al. [62], which we multiply the predicted depth maps by a scalar  $\hat{s}$  to match the median with the groundtruth, i.e.,  $\hat{s} = \text{median}(D_{gt}) / \text{median}(D_{pred})$ .

**Datasets:** We evaluate PhysDepth on three datasets (RobotCar-Night [27], nuScenes-Night [3], and nuScenes-Rain [3])

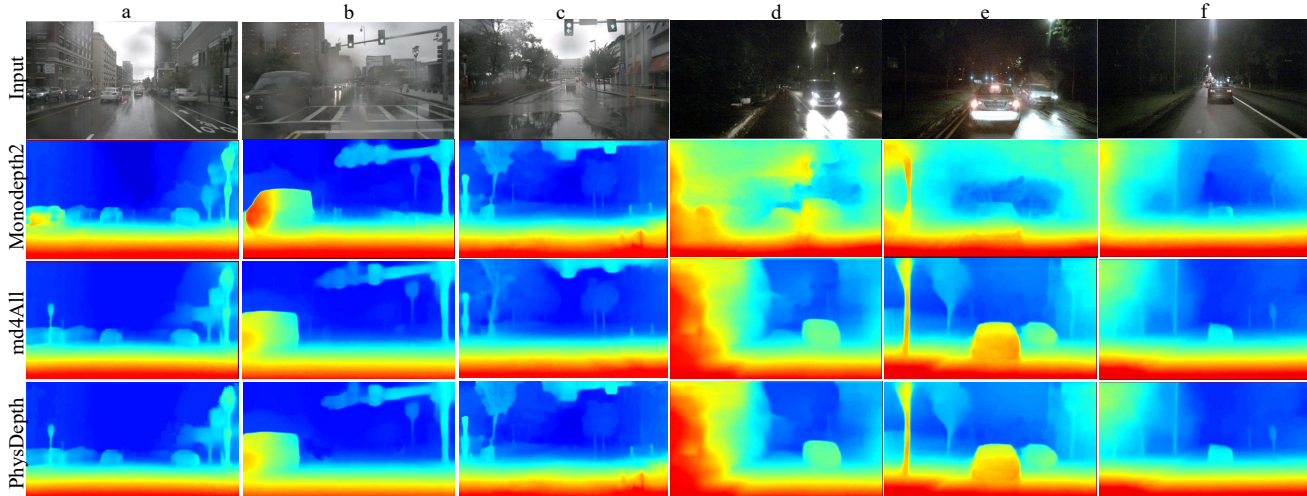


Figure 5. **Qualitative Results - nuScence-Rain and nuScence-Night:** Depth estimated on different test images using PhysDepth and two SOTAs for comparison.

Table 3. **Quantitative Results - nuScenes-Night [3]:** We scale depth up to 80 meters as same as [11, 12]. The best results are in **bold** for each metric. All results presented here are without post-processing. AD and DD mean different training strategies for md4All.

| Methods             | Abs Rel        | RMSE         | $\delta < 1.25$ |
|---------------------|----------------|--------------|-----------------|
|                     | lower's better |              | higher's better |
| STEPS [60]          | 0.474          | 13.158       | 0.334           |
| SRNSD [6]           | 0.352          | 11.942       | 0.419           |
| Robust-Depth [38]   | 0.276          | 10.470       | 0.607           |
| RNW [49]            | 0.290          | 11.289       | 0.557           |
| R4Dyn [11]          | 0.219          | 10.542       | 0.623           |
| DepthDark [56]      | 0.210          | 7.764        | 0.630           |
| Syn2Real-Depth [55] | 0.171          | 7.689        | 0.732           |
| MonoDepth2 [15]     | 0.147          | 6.941        | 0.827           |
| md4All-AD [12]      | 0.182          | 6.372        | 0.753           |
| md4All-DD [12]      | 0.128          | 6.607        | 0.845           |
| <b>PhysDepth</b>    | <b>0.118</b>   | <b>6.349</b> | <b>0.853</b>    |

Table 4. **Quantitative Results - nuScenes-Rain [3]:** We scale depth up to 80 meters as same as [11, 12]. The best results are in **bold** for each metric. All results presented here are without post-processing. AD and DD mean different training strategies for md4All.

| Methods             | Abs Rel        | RMSE         | $\delta < 1.25$ |
|---------------------|----------------|--------------|-----------------|
|                     | lower's better |              | higher's better |
| RNW [45]            | 0.295          | 9.341        | 0.572           |
| R4Dyn [11]          | 0.243          | 10.055       | 0.570           |
| AdaBins [2]         | 0.234          | 7.088        | 0.616           |
| md4All-DD [12]      | 0.214          | 8.376        | 0.680           |
| MonoDepth [24]      | 0.157          | 7.453        | 0.795           |
| md4All-AD [12]      | 0.141          | 6.915        | 0.830           |
| Syn2Real-Depth [55] | 0.133          | 6.926        | 0.817           |
| <b>PhysDepth</b>    | <b>0.130</b>   | <b>6.910</b> | <b>0.835</b>    |

to demonstrate that PhysDepth is accurate and robust under challenging environments. Our model is trained on

those three datasets, respectively.

For baselines, we use any provided training weights from the original authors.

Afterwards, these weights are fine-tuned on all datasets for a fair comparison. More details about the training and testing on the datasets can be found in Section 10 of the Supplementary Material.

We evaluate our proposed model both quantitatively and qualitatively. For quantitative analysis, we perform the comparison against SOTA methods on all three datasets mentioned above. We use three metrics, same as those used in [8, 15] - Abs Rel, RMSE, and  $\delta < 1.25$ . For qualitative analysis, we compare estimated depth maps from PhysDepth and SOTA models using images from RobotCar-Night and nuScenes (night and rain).

#### 4.1. Quantitative Results

Tables 2, 3 show the quantitative results on the Oxford RobotCar-Night, and nuScenes-Night, respectively. As Table 2 and 3 show, our model outperforms all SOTA models across all metrics, emphasizing its overall robustness and accuracy.

This could be attributed to the Physical Prior module and RCA loss, modeling the physical priors of Rayleigh scattering theory and Beer-Lambert law.

These physical prior are more effective than other previously adopted domain-specific features in improving MDE (ADDS [24], and ADFA [45]).

Among Tables 2, 3, md4All [12] and Syn2Real-Depth [55] are two strong baselines, which both adopt GAN-based model and odometry information to achieve better performance.

WSGD [46] uses three techniques to allow the existing photometric loss to work for both day and challenging con-

dition images.

However, either photometric loss or additional constraints still ignore the light attenuation, leading to suboptimal results. Meanwhile, STEPS [60] learns nighttime condition image enhancer to improve nighttime MDE.

R4Dyn [11]’s good performance mainly comes from weak radar supervision. However, PhysDepth outperformed R4Dyn because PhysDepth learns robust physical features while also using weak velocity supervision. RNW [49] is another strong baseline, which performs better than other SOTA by using image enhancement module to enhance image visibility and contrast.

Table 4 provides a quantitative evaluation of our model’s performance on the challenging nuScenes-Rain dataset, demonstrating its robustness to adverse weather conditions. We compare PhysDepth against several SOTA baselines. The results highlight that PhysDepth achieves the best-performing RMSE score of 6.910, Abs Rel of 0.130,  $\delta < 1.25$  of 0.835, significantly outperforming competitors.

Overall, PhysDepth’s high accuracy is attributed to *physical priors: light attenuation for red channel images, which is more robust and effective in improving depth estimation accuracy.*

## 4.2. Qualitative Results

Figure 4 shows results on the RobotCar-Night dataset, qualitatively demonstrating that PhysDepth provides more accurate MDE results under challenging environments. While our depth map clearly delineates the car, ADDS fails to capture its boundary; ADAF and MonoDepth2 detect the car, but their outputs show blurred car boundaries. This is because PhysDepth depends on the red channel, which preserves more complete texture information and minimizes noise from other channels under extremely low-lighting conditions. Moreover, in Figure 4 - c, PhysDepth effectively captures the car’s boundary while other SOTA models all fail to estimate the car’s back windshield area due to low-light and reflection, showcasing PhysDepth’s robustness under challenging environments.

Figure 5 presents a qualitative comparison of our PhysDepth model against SOTA methods Monodepth2 and md4All on challenging test images from the nuScenes-Night and nuScenes-Rain datasets. The top row (Input) displays a variety of challenging conditions, including daytime rain with reflections (a to c) and extreme nighttime glare from headlights (d to f). The subsequent rows visually demonstrate the predicted depth maps from each model, highlighting our method’s ability to produce coherent and stable geometric estimates compared to the baselines under these adverse scenarios.

## 4.3. Plugin Analysis

As discussed before, *PPM and Loss Functions (RCA loss, Weak Velocity Loss, and Photometric Loss)* together serve as a plugin to enhance the accuracy of existing MDE models. Table 5 demonstrates the effectiveness and generality of PhysDepth. We plug in our modules (PPM + Loss Functions) to six SOTA backbones. The results show consistent performance improvements over the baselines on all three datasets across all metrics.

For instance, md4All-AD improves from 0.182 Abs Rel to 0.179 on nuScenes-Night when our module is added. MonoDepth enhanced from 0.453 Abs Rel to 0.448 on RobotCar-Night when plugged in. This robustness generalizes to the nuScenes-Rain dataset, where PhysDepth + RNW (3.791 RMSE) dramatically outperforms the RNW baseline (9.341 RMSE), and PhysDepth + md4All-DD (0.210 Abs Rel) improves over its baseline (0.214 Abs Rel).

The results show that our framework provides a **model-agnostic enhancement** that generalizes from darkness to other challenging low-visibility environments, such as rain.

## 5. Ablation Study

Table 6 presents our core Ablation Study on the RobotCar-Night dataset. We tested four different base architectures: convNeXt-T, MiDaS, ViT-B/16, and ViT-B/32. A clear and consistent trend emerged across all backbones: the baseline models (e.g., ViT-B/16 baseline at 0.678 Abs Rel) performed poorly; adding only the PPM module provided a significant boost (e.g., ViT-B/16+PPM at 0.318 Abs Rel); and finally, adding both the PPM+RCA loss yielded the full, substantial performance gain (e.g., ViT-B/16+PPM+RCA at 0.117 Abs Rel). This strongly demonstrates that both modules are essential and effective, with the ViT-B/32+PPM+RCA combination achieving the overall best results across all metrics (0.114 Abs Rel, 3.522 RMSE, and 0.863  $\delta < 1.25$ ).

In Table 7, our model is trained on channel-specific images from the RobotCar-Night dataset. Those channels are: red channel(R), blue channel(B), green channel(G), and three-channels (RGB). As shown in Table 7, the PhysDepth+R only uses the red channel, which outperforms all other channel/channel-combinations, validating the foundations of our model design: 1) *using red channel images as input*; 2) *adopting physical-prior-knowledge to enhance the accuracy and robustness of MDE.*

Particularly, the findings in Table 7 and in Table 1 are consistent. We can observe that using single-channel image settings (R, G, or B) performs better than using two-channel image (R+G, R+B, or G+B). While using two-channel image settings outperforms using three-channel (RGB) images. This can be attributed to the fact that: *combining multiple channels could introduce noise, especially in low-*

Table 5. **Plug-and-Play Validation and Generalization to Adverse Weather.** We apply our PhysDepth framework as a plug-in module to several existing SOTA models. The results show a consistent performance improvement on RobotCar-Night, nuScenes-Night, and nuScenes-Rain, demonstrating the effectiveness, ‘plug-and-play’ capability, and robustness of our approach against challenging conditions beyond darkness.

| Methods                    | RobotCar-Night |               |                 | nuScenes-Night |               |                 | nuScenes-Rain  |              |                 |
|----------------------------|----------------|---------------|-----------------|----------------|---------------|-----------------|----------------|--------------|-----------------|
|                            | Abs Rel        | RMSE          | $\delta < 1.25$ | Abs Rel        | RMSE          | $\delta < 1.25$ | Abs Rel        | RMSE         | $\delta < 1.25$ |
|                            | lower’s better |               | higher’s better | lower’s better |               | higher’s better | lower’s better |              | higher’s better |
| RNW [45]                   | 0.185          | 6.549         | 0.733           | 0.290          | 11.289        | 0.557           | 0.295          | 9.341        | 0.572           |
| PhysDepth + RNW            | <b>0.180</b>   | <b>6.531</b>  | <b>0.739</b>    | <b>0.286</b>   | <b>11.280</b> | <b>0.562</b>    | <b>0.290</b>   | <b>3.791</b> | <b>0.584</b>    |
| Syn2Real-Depth [55]        | 0.110          | 3.455         | 0.862           | 0.171          | 7.689         | 0.732           | 0.133          | 6.926        | 0.817           |
| PhysDepth + S2R [55]       | <b>0.105</b>   | <b>3.450</b>  | <b>0.869</b>    | <b>0.166</b>   | <b>7.681</b>  | <b>0.737</b>    | <b>0.129</b>   | <b>6.921</b> | <b>0.821</b>    |
| MonoDepth [24]             | 0.453          | 11.420        | 0.700           | 0.147          | 6.941         | 0.827           | 0.157          | 7.453        | 0.795           |
| PhysDepth + MonoDepth [24] | <b>0.448</b>   | <b>11.413</b> | <b>0.708</b>    | <b>0.143</b>   | <b>6.935</b>  | <b>0.823</b>    | <b>0.152</b>   | <b>7.447</b> | <b>0.799</b>    |
| md4All-AD [12]             | 0.124          | 3.612         | 0.858           | 0.182          | 6.372         | 0.753           | 0.141          | 6.915        | 0.830           |
| PhysDepth + md4All-AD [12] | <b>0.119</b>   | <b>3.607</b>  | <b>0.862</b>    | <b>0.179</b>   | <b>6.367</b>  | <b>0.758</b>    | <b>0.137</b>   | <b>6.910</b> | <b>0.836</b>    |
| md4All-DD [12]             | 0.122          | 3.604         | 0.849           | 0.128          | 6.607         | 0.845           | 0.214          | 8.376        | 0.680           |
| PhysDepth + md4All-DD [12] | <b>0.117</b>   | <b>3.600</b>  | <b>0.853</b>    | <b>0.125</b>   | <b>6.601</b>  | <b>0.849</b>    | <b>0.210</b>   | <b>8.371</b> | <b>0.687</b>    |
| DepthDark [56]             | 0.157          | 4.284         | 0.760           | 0.210          | 7.689         | 0.630           | -              | -            | -               |
| PhysDepth+DepthDark [56]   | <b>0.153</b>   | <b>4.280</b>  | <b>0.764</b>    | <b>0.206</b>   | <b>7.683</b>  | <b>0.635</b>    | -              | -            | -               |

Table 6. **Ablation Study - RobotCar-Night [49]:** We evaluate different backbone architectures and module combinations. The best results are in **bold** for each metric.

| Method                  | Abs Rel        | RMSE         | $\delta < 1.25$ |
|-------------------------|----------------|--------------|-----------------|
|                         | lower’s better |              | higher’s better |
| convNeXt-T              | 0.690          | 7.250        | 0.640           |
| convNeXt-T+PPM          | 0.330          | 4.450        | 0.665           |
| convNeXt-T+PPM+RCA      | 0.120          | 3.550        | 0.850           |
| MiDaS                   | 0.671          | 7.098        | 0.651           |
| MiDaS+PPM               | 0.311          | 4.308        | 0.672           |
| MiDaS+PPM+RCA           | 0.118          | 3.529        | 0.858           |
| ViT-B/16                | 0.678          | 7.110        | 0.651           |
| ViT-B/16-T+PPM          | 0.318          | 4.315        | 0.675           |
| <b>ViT-B/16+PPM+RCA</b> | <b>0.117</b>   | <b>3.525</b> | <b>0.860</b>    |
| ViT-B/32                | 0.675          | 7.105        | 0.655           |
| ViT-B/32+PPM            | 0.314          | 4.310        | 0.678           |
| <b>ViT-B/32+PPM+RCA</b> | <b>0.114</b>   | <b>3.522</b> | <b>0.863</b>    |

Table 7. **Ablation Study of Using Different Channel Images on RobotCar-Night Dataset [27]:** R means Red Channel, so do B (Blue Channel) and G (Green Channel), RGB. The best results are in **bold**.

| Methods            | Abs Rel        | RMSE         |
|--------------------|----------------|--------------|
|                    | lower’s better |              |
| PhysDepth+RGB      | 0.171          | 4.028        |
| PhysDepth+B+R      | 0.155          | 3.921        |
| PhysDepth+G+R      | 0.156          | 3.897        |
| PhysDepth+B+G      | 0.159          | 3.842        |
| PhysDepth+B        | 0.120          | 3.540        |
| PhysDepth+G        | 0.119          | 3.531        |
| <b>PhysDepth+R</b> | <b>0.117</b>   | <b>3.525</b> |

*light conditions* (e.g., Green and Blue channels tend to lose more texture information due to Rayleigh Scattering theory). That is, the additional channels (Green and Blue), instead of contributing significantly useful image information, could “noise” the primary channel (Red) and confuse

depth estimation models, leading to compromised MDE results. Additionally, the red channel performs best among all single-channel settings, followed by the green channel; the blue channel performs the worst. The results yield with Rayleigh scattering theory (Equation 2) that  $I_{red} < I_{green} < I_{blue}$ , which  $I$  represents intensity of scattering.

Table 8. **Ablation Study of Attenuation Item:** Using red channel images from the RobotCar-Night dataset [49] and the depth range is up to 80m. Linear means that we treat light attenuation as a linear function. And so do Quadratic and Exponential. The best results are in **bold**.

| Methods                      | Abs Rel        | RMSE         |
|------------------------------|----------------|--------------|
|                              | lower’s better |              |
| PhysDepth+Linear             | 0.122          | 3.741        |
| PhysDepth+Quadratic          | 0.129          | 3.735        |
| <b>PhysDepth+Exponential</b> | <b>0.121</b>   | <b>3.657</b> |

We also conduct a study of attenuation item  $e^{-\mu d_R}$  (Exponential) in Table 8. While the other parts in Equation 3 remain the same, we first change  $e^{-\mu d_R}$  to linear function (Equation 8). And then, we change  $e^{-\mu d_R}$  to quadratic function (Equation 9). For the experiment settings, we set  $a = 0.0095, b = 0.05$  for Equation 8 [20]. We then set  $a = 0.0095, b = 0.05, c = 1.0$  for Equation 9 [20]. All other experiment settings stay the same as in Table 2. The results demonstrate our design choice of using  $e^{-\mu d_R}$  as attenuation item.

The supplementary material includes additional results and discussions, such as an ablation study on various light attenuation functions, analyses of different depth ranges, additional qualitative results, failure cases, etc.

## 6. Conclusion and Limitations

In this work, we identify a critical weakness in modern monocular depth estimation, and demonstrate that SOTA models often fail in challenging environments by overlooking physical information. We substantiate this claim through an empirical study. We propose PhysDepth, a novel, plug-and-play framework designed to infuse physical priors into existing MDE backbones.

Extensive quantitative and qualitative evaluations on the RobotCar-Night, nuScenes-Night, and nuScenes-Rain datasets demonstrate that PhysDepth achieves SOTA accuracy. Furthermore, we validate the generality and model-agnostic nature of our approach. By applying PhysDepth as a plugin to multiple existing SOTA backbones, we observe consistent and significant performance improvements, confirming its utility as a plug-and-play solution.

While PhysDepth demonstrates remarkable robustness, we acknowledge limitations in extreme scenarios, such as severe halos from direct headlights, which can corrupt the attenuation signal. Future work will focus on explicitly modeling these complex lighting phenomena. Ultimately, PhysDepth validates a new, physically-grounded paradigm for MDE, paving the way for next-generation models that can operate reliably in the challenging conditions of the real world.

## References

- [1] Jimmy Lei Ba, Jamie Ryan Kiros, and Geoffrey E Hinton. Layer normalization. *arXiv preprint arXiv:1607.06450*, 2016. 2
- [2] Shariq Farooq Bhat, Ibraheem Alhashim, and Peter Wonka. Adabins: Depth estimation using adaptive bins. In *Proceedings of the IEEE/CVF Conference on Computer Vision and Pattern Recognition*, pages 4009–4018, 2021. 6
- [3] Holger Caesar, Varun Bankiti, Alex H Lang, Sourabh Vora, Venice Erin Liong, Qiang Xu, Anush Krishnan, Yu Pan, Giancarlo Baldan, and Oscar Beijbom. nuscenes: A multi-modal dataset for autonomous driving. In *Proceedings of the IEEE/CVF conference on computer vision and pattern recognition*, pages 11621–11631, 2020. 5, 6, 2, 3
- [4] Younjoon Chung, Hyoungseob Park, Patrick Rim, Xiaoran Zhang, Jihe He, Ziyao Zeng, Safa Cicek, Byung-Woo Hong, James S. Duncan, and Alex Wong. Eta: Energy-based test-time adaptation for depth completion. In *Proceedings of the IEEE/CVF International Conference on Computer Vision (ICCV)*, pages 6001–6012, 2025. 2
- [5] Runmin Cong, Chunlei Wu, Xibin Song, Wei Zhang, Sam Kwong, Hongdong Li, and Pan Ji. Srnsd: Structure-regularized night-time self-supervised monocular depth estimation for outdoor scenes. *IEEE Transactions on Image Processing*, 33:5538–5550, 2024. 2
- [6] Runmin Cong, Chunlei Wu, Xibin Song, Wei Zhang, Sam Kwong, Hongdong Li, and Pan Ji. Srnsd: Structure-regularized night-time self-supervised monocular depth estimation for outdoor scenes. *IEEE Transactions on Image Processing*, 2024. 6, 3
- [7] Xingshuai Dong, Matthew A Garratt, Sreenatha G Annavatti, and Hussein A Abbass. Towards real-time monocular depth estimation for robotics: A survey. *IEEE Transactions on Intelligent Transportation Systems*, 23(10):16940–16961, 2022. 1
- [8] David Eigen, Christian Puhrsch, and Rob Fergus. Depth map prediction from a single image using a multi-scale deep network. *Advances in neural information processing systems*, 27, 2014. 6
- [9] Raanan Fattal. Single image dehazing. In *ACM SIGGRAPH 2008 Papers*, New York, NY, USA, 2008. Association for Computing Machinery. 2
- [10] Ziyue Feng, Liang Yang, Longlong Jing, Haiyan Wang, YingLi Tian, and Bing Li. Disentangling object motion and occlusion for unsupervised multi-frame monocular depth. In *Computer Vision – ECCV 2022*, pages 228–244, Cham, 2022. Springer Nature Switzerland. 6
- [11] Stefano Gasperini, Patrick Koch, Vinzenz Dallabetta, Nassir Navab, Benjamin Busam, and Federico Tombari. R4dyn: Exploring radar for self-supervised monocular depth estimation of dynamic scenes. In *2021 International Conference on 3D Vision (3DV)*, pages 751–760. IEEE, 2021. 2, 6, 7
- [12] Stefano Gasperini, Nils Morbitzer, HyunJun Jung, Nassir Navab, and Federico Tombari. Robust monocular depth estimation under challenging conditions. In *Proceedings of the IEEE/CVF International Conference on Computer Vision*, pages 8177–8186, 2023. 1, 2, 3, 5, 6, 8, 7
- [13] Andreas Geiger, Philip Lenz, and Raquel Urtasun. Are we ready for autonomous driving? the kitti vision benchmark suite. In *2012 IEEE Conference on Computer Vision and Pattern Recognition*, pages 3354–3361. IEEE, 2012. 6
- [14] Clément Godard, Oisín Mac Aodha, and Gabriel J Brostow. Unsupervised monocular depth estimation with left-right consistency. In *Proceedings of the IEEE conference on computer vision and pattern recognition*, pages 270–279, 2017. 5
- [15] Clément Godard, Oisín Mac Aodha, Michael Firman, and Gabriel J Brostow. Digging into self-supervised monocular depth estimation. In *Proceedings of the IEEE/CVF international conference on computer vision*, pages 3828–3838, 2019. 1, 2, 5, 6, 4
- [16] Vitor Guizilini, Rares Ambrus, Sudeep Pillai, Allan Ravenstos, and Adrien Gaidon. 3d packing for self-supervised monocular depth estimation. In *Proceedings of the IEEE/CVF conference on computer vision and pattern recognition*, pages 2485–2494, 2020. 5, 2
- [17] Kaiming He, Jian Sun, and Xiaoou Tang. Single image haze removal using dark channel prior. *IEEE transactions on pattern analysis and machine intelligence*, 33(12):2341–2353, 2010. 2
- [18] Mingbo Hong, Shen Cheng, Haibin Huang, Haoqiang Fan, and Shuaicheng Liu. You only look around: Learning illumination invariant feature for low-light object detection. *Advances in Neural Information Processing Systems*, 2024. 4

- [19] Shengyu Hou, Mengyin Fu, Rongchuan Wang, Yi Yang, and Wenjie Song. Self-supervised monocular depth estimation for all-day images based on dual-axis transformer. *IEEE Transactions on Circuits and Systems for Video Technology*, 34(10):9939–9953, 2024. 2
- [20] <https://wiki.ogre3d.org/>. Point light attenuation, 2011. 8
- [21] Diederik P Kingma and Jimmy Ba. Adam: A method for stochastic optimization. *arXiv preprint arXiv:1412.6980*, 2014. 5
- [22] Zhengqin Li, Jia Shi, Sai Bi, Rui Zhu, Kalyan Sunkavalli, Miloš Hašan, Zexiang Xu, Ravi Ramamoorthi, and Manmohan Chandraker. Physically-based editing of indoor scene lighting from a single image. In *European Conference on Computer Vision*, pages 555–572. Springer, 2022. 4
- [23] Zhenyu Li, Zehui Chen, Xianming Liu, and Junjun Jiang. Depthformer: Exploiting long-range correlation and local information for accurate monocular depth estimation. *Machine Intelligence Research*, 20(6):837–854, 2023. 6
- [24] Lina Liu, Xibin Song, Mengmeng Wang, Yong Liu, and Liangjun Zhang. Self-supervised monocular depth estimation for all day images using domain separation. In *Proceedings of the IEEE/CVF international conference on computer vision*, pages 12737–12746, 2021. 1, 2, 5, 6, 8
- [25] Zhuang Liu, Hanzi Mao, Chao-Yuan Wu, Christoph Feichtenhofer, Trevor Darrell, and Saining Xie. A convnet for the 2020s. In *Proceedings of the IEEE/CVF conference on computer vision and pattern recognition*, pages 11976–11986, 2022. 3, 4
- [26] Yawen Lu and Guoyu Lu. An alternative of lidar in nighttime: Unsupervised depth estimation based on single thermal image. In *Proceedings of the IEEE/CVF Winter Conference on Applications of Computer Vision*, pages 3833–3843, 2021. 2
- [27] Will Maddern, Geoffrey Pascoe, Chris Linegar, and Paul Newman. 1 year, 1000 km: The oxford robotcar dataset. *Int. J. Rob. Res.*, 36(1):3–15, 2017. 3, 4, 5, 8
- [28] Jaeho Moon, Juan Luis Gonzalez Bello, Byeongjun Kwon, and Munchurl Kim. From-ground-to-objects: Coarse-to-fine self-supervised monocular depth estimation of dynamic objects with ground contact prior. In *Proceedings of the IEEE/CVF Conference on Computer Vision and Pattern Recognition*, pages 10519–10529, 2024. 6
- [29] Srinivasa G Narasimhan and Shree K Nayar. Chromatic framework for vision in bad weather. In *Proceedings IEEE Conference on Computer Vision and Pattern Recognition. CVPR 2000 (Cat. No. PR00662)*, pages 598–605. IEEE, 2000. 2
- [30] Srinivasa G Narasimhan and Shree K Nayar. Vision and the atmosphere. *International journal of computer vision*, 48(3): 233–254, 2002. 2
- [31] Dennis Park, Rares Ambrus, Vitor Guizilini, Jie Li, and Adrien Gaidon. Is pseudo-lidar needed for monocular 3d object detection? In *Proceedings of the IEEE/CVF International Conference on Computer Vision*, pages 3142–3152, 2021. 1
- [32] Juhyung Park, Woojin Jung, Eun-Jung Choi, Se-Hong Oh, Jinhee Jang, Dongmyung Shin, Hongjun An, and Jongho Lee. Diffnet: Diffusion parameter mapping network generalized for input diffusion gradient schemes and b-value. *IEEE Transactions on Medical Imaging*, 41(2):491–499, 2021. 6
- [33] Adam Paszke, Sam Gross, Francisco Massa, Adam Lerer, James Bradbury, Gregory Chanan, Trevor Killeen, Zeming Lin, Natalia Gimelshein, Luca Antiga, Alban Desmaison, Andreas Köpf, Edward Yang, Zach DeVito, Martin Raison, Alykhan Tejani, Sasank Chilamkurthy, Benoit Steiner, Lu Fang, Junjie Bai, and Soumith Chintala. Pytorch: an imperative style, high-performance deep learning library. In *Proceedings of the 33rd International Conference on Neural Information Processing Systems*, Red Hook, NY, USA, 2019. Curran Associates Inc. 5
- [34] Rui Peng, Ronggang Wang, Yawen Lai, Luyang Tang, and Yangang Cai. Excavating the potential capacity of self-supervised monocular depth estimation. In *Proceedings of the IEEE/CVF International Conference on Computer Vision*, pages 15560–15569, 2021. 6
- [35] Luigi Piccinelli, Yung-Hsu Yang, Christos Sakaridis, Mattia Segu, Siyuan Li, Luc Van Gool, and Fisher Yu. Unidepth: Universal monocular metric depth estimation. In *Proceedings of the IEEE/CVF Conference on Computer Vision and Pattern Recognition*, pages 10106–10116, 2024. 3, 2
- [36] Uchitha Rajapaksha, Ferdous Sohel, Hamid Laga, Dean Diepeveen, and Mohammed Bennamoun. Deep learning-based depth estimation methods from monocular image and videos: A comprehensive survey. *ACM Computing Surveys*, 56(12):1–51, 2024. 1
- [37] René Ranftl, Katrin Lasinger, David Hafner, Konrad Schindler, and Vladlen Koltun. Towards robust monocular depth estimation: Mixing datasets for zero-shot cross-dataset transfer. *IEEE transactions on pattern analysis and machine intelligence*, 44(3):1623–1637, 2020. 3
- [38] Kieran Saunders, George Vogiatzis, and Luis J Manso. Self-supervised monocular depth estimation: Let’s talk about the weather. In *Proceedings of the IEEE/CVF International Conference on Computer Vision*, pages 8907–8917, 2023. 6
- [39] Aashish Sharma, Loong-Fah Cheong, Lionel Heng, and Robby T Tan. Nighttime stereo depth estimation using joint translation-stereo learning: Light effects and uninformative regions. In *2020 International Conference on 3D Vision (3DV)*, pages 23–31. IEEE, 2020. 2
- [40] Chang Shu, Kun Yu, Zhixiang Duan, and Kuiyuan Yang. Feature-metric loss for self-supervised learning of depth and egomotion. In *European Conference on Computer Vision*, pages 572–588. Springer, 2020. 6
- [41] Jaime Spencer, Richard Bowden, and Simon Hadfield. Defeat-net: General monocular depth via simultaneous unsupervised representation learning. In *Proceedings of the IEEE/CVF Conference on Computer Vision and Pattern Recognition*, pages 14402–14413, 2020. 1, 2, 5, 6
- [42] Robby T Tan. Visibility in bad weather from a single image. In *2008 IEEE conference on computer vision and pattern recognition*, pages 1–8. IEEE, 2008. 2
- [43] Phan Thi Huyen Thanh, Minh Huy Vu Nguyen, Trung Thai Tran, Tran Vu Pham, Duc Dung Nguyen, Truong Vinh Truong Duy, Natori Naotake, et al. Depthsegnet24:

- A label-free model for robust day-night depth and semantics. In *Proceedings of the Asian Conference on Computer Vision*, pages 2716–2733, 2024. 5
- [44] Benjamin Ummenhofer, Huizhong Zhou, Jonas Uhrig, Nikolaus Mayer, Eddy Ilg, Alexey Dosovitskiy, and Thomas Brox. Demon: Depth and motion network for learning monocular stereo. In *Proceedings of the IEEE conference on computer vision and pattern recognition*, pages 5038–5047, 2017. 4
- [45] Madhu Vankadari, Sourav Garg, Anima Majumder, Swagat Kumar, and Ardhendu Behera. Unsupervised monocular depth estimation for night-time images using adversarial domain feature adaptation. In *European Conference on Computer Vision*, pages 443–459. Springer, 2020. 1, 2, 5, 6, 8
- [46] Madhu Vankadari, Stuart Golodetz, Sourav Garg, Sangyun Shin, Andrew Markham, and Niki Trigoni. When the sun goes down: Repairing photometric losses for all-day depth estimation. In *Conference on Robot Learning*, pages 1992–2003. PMLR, 2023. 2, 3, 5, 6
- [47] Madhu Vankadari, Samuel Hodgson, Sangyun Shin, Kaichen Zhou, Andrew Markham, and Niki Trigoni. Dusk till dawn: Self-supervised nighttime stereo depth estimation using visual foundation models. In *2024 IEEE International Conference on Robotics and Automation (ICRA)*, pages 17976–17982. IEEE, 2024. 1
- [48] Jiaping Wang, Peiran Ren, Minmin Gong, John Snyder, and Baining Guo. All-frequency rendering of dynamic, spatially-varying reflectance. *ACM Trans. Graph.*, 28(5):1–10, 2009. 4
- [49] Kun Wang, Zhenyu Zhang, Zhiqiang Yan, Xiang Li, Baobei Xu, Jun Li, and Jian Yang. Regularizing nighttime weirdness: Efficient self-supervised monocular depth estimation in the dark. In *Proceedings of the IEEE/CVF international conference on computer vision*, pages 16055–16064, 2021. 1, 2, 3, 5, 6, 7, 8, 4
- [50] Ruoyu Wang, Zehao Yu, and Shenghua Gao. Planedepth: Self-supervised depth estimation via orthogonal planes. In *Proceedings of the IEEE/CVF Conference on Computer Vision and Pattern Recognition*, pages 21425–21434, 2023. 6
- [51] Yan Wang, Wei-Lun Chao, Divyansh Garg, Bharath Hariharan, Mark Campbell, and Kilian Q Weinberger. Pseudolidar from visual depth estimation: Bridging the gap in 3d object detection for autonomous driving. In *Proceedings of the IEEE/CVF conference on computer vision and pattern recognition*, pages 8445–8453, 2019. 1
- [52] Zian Wang, Jonah Philion, Sanja Fidler, and Jan Kautz. Learning indoor inverse rendering with 3d spatially-varying lighting. In *Proceedings of the IEEE/CVF International Conference on Computer Vision*, pages 12538–12547, 2021. 4
- [53] Jiaying Yan, Hong Zhao, Penghui Bu, and YuSheng Jin. Channel-wise attention-based network for self-supervised monocular depth estimation. In *2021 International Conference on 3D Vision (3DV)*, pages 464–473. IEEE, 2021. 6
- [54] Weilong Yan, Ming Li, Haipeng Li, Shuwei Shao, and Robby T. Tan. Synthetic-to-real self-supervised robust depth estimation via learning with motion and structure priors. In *Proceedings of the IEEE/CVF Conference on Computer Vision and Pattern Recognition (CVPR)*, pages 21880–21890, 2025. 2
- [55] Weilong Yan, Ming Li, Haipeng Li, Shuwei Shao, and Robby T Tan. Synthetic-to-real self-supervised robust depth estimation via learning with motion and structure priors. In *Proceedings of the Computer Vision and Pattern Recognition Conference*, pages 21880–21890, 2025. 5, 6, 8
- [56] Longjian Zeng, Zunjie Zhu, Rongfeng Lu, Ming Lu, Bolun Zheng, Chenggang Yan, and Anke Xue. Depthdark: Robust monocular depth estimation for low-light environments. In *Proceedings of the 33rd ACM International Conference on Multimedia*, pages 11239–11248, 2025. 3, 5, 6, 8
- [57] Junding Zhang, Di Rao, Youssef Akoudad, Wei Gao, and Jie Chen. Lightweight self-supervised monocular depth estimation for all-day scenes using generative adversarial network. In *ICASSP 2025-2025 IEEE International Conference on Acoustics, Speech and Signal Processing (ICASSP)*, pages 1–5. IEEE, 2025. 2
- [58] Wenyao Zhang, Hongsi Liu, Bohan Li, Jiawei He, Zekun Qi, Yunnan Wang, Shengyang Zhao, Xinqiang Yu, Wenjun Zeng, and Xin Jin. Hybrid-grained feature aggregation with coarse-to-fine language guidance for self-supervised monocular depth estimation. In *Proceedings of the IEEE/CVF International Conference on Computer Vision (ICCV)*, pages 6678–6692, 2025. 2
- [59] Chaoqiang Zhao, Yang Tang, and Qiyu Sun. Unsupervised monocular depth estimation in highly complex environments. *IEEE Transactions on Emerging Topics in Computational Intelligence*, 6(5):1237–1246, 2022. 2
- [60] Yupeng Zheng, Chengliang Zhong, Pengfei Li, Huan-ang Gao, Yuhang Zheng, Bu Jin, Ling Wang, Hao Zhao, Guyue Zhou, Qichao Zhang, and Dongbin Zhao. Steps: Joint self-supervised nighttime image enhancement and depth estimation. In *2023 IEEE International Conference on Robotics and Automation (ICRA)*, pages 4916–4923, 2023. 1, 3, 5, 6, 7
- [61] Brady Zhou, Philipp Krähenbühl, and Vladlen Koltun. Does computer vision matter for action? *Science Robotics*, 4(30):eaaw6661, 2019. 1
- [62] Tinghui Zhou, Matthew Brown, Noah Snavely, and David G Lowe. Unsupervised learning of depth and ego-motion from video. In *Proceedings of the IEEE conference on computer vision and pattern recognition*, pages 1851–1858, 2017. 5, 1, 2, 4, 6

# PhysDepth: Plug-and-Play Physical Refinement for Monocular Depth Estimation in Challenging Environments

## Supplementary Material

### 7. Supplementary Material Introduction

This appendix includes additional details and results to support our manuscript. In particular, this appendix is organized as follows:

- In Section 8, we provide the formal pseudocode detailing the step-by-step computation of covariance  $Cov$  between a model’s error metric and atmosphere attenuation  $\beta$
- In Section 9, we discuss more details about the PhysDepth
- In Section 10, we discuss more details about the datasets.
- In Section 11, we show more quantitative results.
- In Section 12, we present additional qualitative results.
- In Section 13, we verify the performance of PhysDepth on daytime dataset.
- In Section 14, we review failure cases.

### 8. Covariance Computation

This section presents Algorithm 1, which provides the pseudocode detailing the step-by-step computation of the Covariance used in our empirical study.

**Rationale and Hypothesis.** Our core hypothesis is that a model’s response to controlled attenuation reveals its underlying strategy:

1) Heuristic-Follower (Non-Physical): A model that relies on simple heuristics (e.g., "brighter light = closer") or texture cues will perceive attenuation as noise. As the attenuation coefficient increases, its primary cues are destroyed, and its prediction error will increase.

2) Physics-Informed (Physical): A model that has learned to invert the Beer-Lambert law will treat attenuation as a signal. As the attenuation coefficient increases, it gains a stronger, valid cue for depth (i.e., it correctly identifies that dimmer objects, relative to their known class, are farther away), and its prediction error will remain stable or decrease.

**Ablation for Covariance:** A potential flaw of the Covariance is that it may unfairly favor our model, which is trained on a loss derived from the same physical law. To disentangle the contribution of our RCA loss from the simpler effect of merely exposing the model to attenuated images, we conduct a crucial ablation study. We compare three models:

- Model A (Baseline): The standard ViT-B/32 model trained with only the photometric loss.
- Model B (Augment-Only): The baseline ViT-B/32 model trained with the Eq. (1) applied as a random data augmentation.

- Model C (Ours): Our full PhysDepth model ( ViT-B/32+ PPM + RCA), trained with our proposed RCA loss but without covariance augmentation.

We then set  $\beta = 0.025$  and evaluate all three models on the Covariance, with results in Table 9. It clearly demonstrates the limitation of non-physical approaches. The Baseline (Model A) is brittle, with a positive Covariance of +0.180. Applying data augmentation (Model B) provides some robustness, lowering the score to +0.142, but the model’s strategy remains "brittle" ( $Cov > 0$ ), as it still treats attenuation as noise. In sharp contrast, our full model (Model C) achieves a score of  $-0.040$ . This result is critical for two reasons: 1. The score is negative ( $Cov < 0$ ). It demonstrates that our model has successfully learned to invert the Beer-Lambert law and use attenuation as a valid (albeit subtle) signal for depth, aligning with the "Physics-Informed" strategy. The score is near-zero ( $Cov \approx 0.0$ ), which proves our model has also learned a near-perfectly robust and decoupled strategy, performing invariantly to attenuation. This is the paper’s key finding: simple data augmentation (Model B) can only learn some invariance, and its strategy remains brittle (positive score). Our RCA loss forces the model to learn the true underlying physical principle, proven by its ability to achieve a robust, negative-scoring strategy.

Table 9. Ablation study isolating the contribution of the RCA loss. We compare Covariance across three models: (A) the baseline, (B) the baseline trained with Covariance perturbations as data augmentation, and (C) our full model with the RCA loss. The negative score for our model demonstrates it has learned to invert the attenuation, while others still treat it as noise.

| Method                 | RCA Loss | Cov Augment. | Cov (AbsRel) |
|------------------------|----------|--------------|--------------|
| Model A (Baseline)     | ×        | ×            | +0.180       |
| Model B (Augment-Only) | ×        | ✓            | +0.142       |
| Model C (Ours)         | ✓        | ×            | -0.040       |

### 9. PhysDepth Design

In our base MDE model, the encoder is followed by a self-attention and a series of convolutional upsampling layers to form the decoder. Regarding the prediction layers, like Zhou et al. [62], we use  $\frac{1}{\alpha \cdot \text{Sigmoid}(x) + \beta}$  with  $\alpha = 10$  and  $\beta = 0.0125$  to constrain the predicted depth to be always positive within a reasonable range (e.g., 80 meters). In addition, we use a Self-Attention module between the encoder and decoder to further improve the accuracy of the baseline.

---

**Algorithm 1** Covariance Computation Computation

---

**Require:** MDE model  $M$

**Require:** Test dataset  $\mathcal{D} = \{(I^{(j)}, D_{gt}^{(j)})\}_{j=1}^K$

**Require:** Perturbation vector  $\mathbf{B} = [\beta_0, \dots, \beta_N]$  (extinction coefficients)

**Require:** Nocturnal Airlight  $A$  (e.g.,  $[0.1, 0.1, 0.1]$ ), Error function  $\text{Error}(\cdot, \cdot)$  (AbsRel)

**Require:** Average Covariance score  $\overline{\text{Cov}}$

```
1: Initialize score_list  $\leftarrow []$ 
2: for each  $(I^{(j)}, D_{gt}^{(j)}) \in \mathcal{D}$  do ▷ Loop over all K images in test set
3:   Initialize error vector  $\mathbf{E}^{(j)} \leftarrow []$ 
4:   for each  $\beta_i \in \mathbf{B}$  do ▷ Loop over N perturbation levels ▷ Step 1: Generate Perturbed Image
5:      $t_i \leftarrow \exp(-\beta_i \cdot D_{gt}^{(j)})$  ▷ Calculate transmission map
6:      $I'_i \leftarrow I^{(j)} \cdot t_i + A \cdot (1 - t_i)$  ▷ Synthesize attenuated image
7:      $D_{pred,i} \leftarrow M(I'_i)$  ▷ Step 2: Model Inference
8:      $\mathcal{E}_i \leftarrow \text{Error}(D_{pred,i}, D_{gt}^{(j)})$  ▷ Get model's prediction
9:     Append  $\mathcal{E}_i$  to  $\mathbf{E}^{(j)}$  ▷ Step 3: Calculate Error
10:  end for ▷ Step 4: Compute Score for image  $j$ 
11:   $\rho_j \leftarrow \text{PearsonCorrelation}(\mathbf{B}, \mathbf{E}^{(j)})$  ▷  $\rho(\mathbf{B}, \mathbf{E}^{(j)})$ 
12:  Append  $\rho_j$  to score_list
13: end for
14:  $\overline{\text{Cov}} \leftarrow \text{Mean}(\text{score\_list})$  ▷ Average score over all images
15: return  $\overline{\text{Cov}}$ 
```

---

**Encoder:** Following follow Piccinelli et al. [35], for ViT and ConvNeXt we remove all classification-specific layers (e.g., global pooling, fully connected, and softmax) from each. Then we first take the encoder output, flatten it, and apply LayerNorm [1]. We then project the feature to a 1024-dimensional channel space using a linear layer and bilinearly interpolate the result to a same resolution of H and W as ViT encoder’s output dimension

**Pose Estimation CNN:** The pose estimation network learns a pose transformation between two consecutive frames, which serves as a part of our self-supervised signals for depth estimation. We follow the same network in SfMLearner [62], in which we concatenate two consecutive frames along the channel direction. The concatenated result is fed into the Pose Estimation CNN. The outputs are the relative poses between each of the source views and the target view. Specifically, the network consists of 2 convolutions followed by a  $1 \times 1$  convolution with  $6 \times 1$  output channels. One channel corresponds to 3 Euler angles and a 3-D translation for each source view. All convolution layers are followed by ReLU except for the last layer, where no nonlinear activation is applied. Since we use photometric reconstruction loss function  $\mathcal{L}_p$  from SfMLearner [62] during the training processes, which implies that the rigid assumptions in SfMLearner [62] also apply to our model.

**Weak Velocity Supervision:** We follow [12, 16] to use

a weak velocity supervision  $\mathcal{L}_v$  for scale awareness and ensure consistent predictions when the photometric consistency does not hold.  $\mathcal{L}_v$  is defined in Equation 7

$$\mathcal{L}_v(\hat{T}_{t \rightarrow s}, T_{t \rightarrow s}) = \left| \|\hat{T}_{t \rightarrow s}\|_2 - \|T_{t \rightarrow s}\|_2 \right| \quad (7)$$

$\hat{T}_{t \rightarrow s}$  and  $T_{t \rightarrow s}$  are the predicted and ground truth pose translations, respectively. We can easily obtain them from the available odometry information, through the ego vehicle speed and the time interval across frames.

## 10. Data Set Details

**Oxford RobotCar-Night:** The RobotCar-Night dataset contains images from the 2014-12-16-18-44-24 folder, which includes 6000 training images and 411 test images. All images are cropped to  $1152 \times 672$ .

**nuScenes-Night and nuScenes-Rain:** From the original nuScenes dataset [3], Wang et al. [49] created the nuScenes-Night dataset split, which contains over 10000 training images and 500 test samples. All images are cropped to  $1536 \times 768$ . All images are in  $1242 \times 375$ .

Table 10. **Ablation Study:** We test PhysDepth and Plugin-enhanced Models on all images from nuScenes-Night dataset [3] in 40 meters depth range. The best results are in **bold**.

|                              | Methods             | Abs Rel<br>lower's better | RMSE         | $\delta < 1.25$<br>higher's better |
|------------------------------|---------------------|---------------------------|--------------|------------------------------------|
| SOTA                         | Monodepth2          | 0.116                     | 3.701        | 0.876                              |
|                              | md4All-AD           | 0.121                     | 3.851        | 0.870                              |
|                              | md4All-DD           | 0.109                     | 3.606        | 0.883                              |
| Plugin<br>Enhanced<br>Models | PhysDepth+DepthDark | 0.111                     | 3.595        | 0.905                              |
|                              | PhysDepth+ConvNeXt  | 0.107                     | 3.593        | 0.908                              |
|                              | PhysDepth+S2R       | 0.103                     | 3.591        | 0.910                              |
|                              | PhysDepth+ViT-B/16  | 0.101                     | 3.589        | 0.908                              |
| Ours                         | <b>PhysDepth</b>    | <b>0.098</b>              | <b>3.586</b> | <b>0.906</b>                       |

Table 11. **Ablation Study:** We test PhysDepth and Plugin-enhanced Models on all images from nuScenes-Night dataset [3] in 50 meters depth range. The best results are in **bold**.

|                              | Methods             | Abs Rel<br>lower's better | RMSE         | $\delta < 1.25$<br>higher's better |
|------------------------------|---------------------|---------------------------|--------------|------------------------------------|
| SOTA                         | Monodepth2          | 0.136                     | 5.645        | 0.869                              |
|                              | md4All-AD           | 0.131                     | 5.728        | 0.865                              |
|                              | md4All-DD           | 0.122                     | 5.413        | 0.876                              |
| Plugin<br>Enhanced<br>Models | PhysDepth+DepthDark | 0.115                     | 5.417        | 0.874                              |
|                              | PhysDepth+ConvNeXt  | 0.117                     | 5.416        | 0.872                              |
|                              | PhysDepth+S2R       | 0.116                     | 5.415        | 0.872                              |
|                              | PhysDepth+ViT-B/16  | 0.113                     | 5.414        | 0.876                              |
| Ours                         | <b>PhysDepth</b>    | <b>0.111</b>              | <b>5.411</b> | <b>0.878</b>                       |

Table 12. **Ablation Study:** We test PhysDepth and Plugin-enhanced Models on all images from nuScenes-Night dataset [3] in 60 meters depth range. The best results are in **bold**.

|                              | Methods             | Abs Rel<br>lower's better | RMSE         | $\delta < 1.25$<br>higher's better |
|------------------------------|---------------------|---------------------------|--------------|------------------------------------|
| SOTA                         | Monodepth2          | 0.137                     | 5.650        | 0.841                              |
|                              | md4All-AD           | 0.135                     | 5.731        | 0.841                              |
|                              | md4All-DD           | 0.122                     | 5.418        | 0.855                              |
| Plugin<br>Enhanced<br>Models | PhysDepth+DepthDark | 0.120                     | 5.424        | 0.857                              |
|                              | PhysDepth+ConvNeXt  | 0.124                     | 5.427        | 0.854                              |
|                              | PhysDepth+S2R       | 0.118                     | 5.420        | 0.859                              |
|                              | PhysDepth+ViT-B/16  | 0.117                     | 5.418        | 0.861                              |
| Ours                         | <b>PhysDepth</b>    | <b>0.115</b>              | <b>5.415</b> | <b>0.863</b>                       |

Table 13. **Ablation Study:** PhysDepth and Plugin-enhanced Models on all images from the RobotCar-Night dataset [49] and set depth range up to 40 meters. The best results are in **bold**.

|                              | Methods             | Abs Rel<br>lower's better | RMSE         | $\delta < 1.25$<br>higher's better |
|------------------------------|---------------------|---------------------------|--------------|------------------------------------|
| SOTA                         | Monodepth2          | 0.302                     | 4.984        | 0.461                              |
|                              | md4All-AD           | 0.120                     | 3.531        | 0.859                              |
|                              | md4All-DD           | 0.121                     | 3.479        | 0.849                              |
| Plugin<br>Enhanced<br>Models | PhysDepth+DepthDark | 0.125                     | 3.470        | 0.847                              |
|                              | PhysDepth+ConvNeXt  | 0.121                     | 3.467        | 0.884                              |
|                              | PhysDepth+S2R       | 0.125                     | 3.471        | 0.844                              |
|                              | PhysDepth+ViT-B/16  | 0.112                     | 3.468        | 0.850                              |
| Ours                         | <b>PhysDepth</b>    | <b>0.107</b>              | <b>3.445</b> | <b>0.887</b>                       |

## 11. Additional Quantitative Results

### 11.1. Evaluation over Different Distances

Table 10, 11, and 12 are the results of nuScenes-Night dataset [3] with different depth scales. Specifically, we al-

Table 14. **Ablation Study:** PhysDepth and Plugin-enhanced Models on all images from the RobotCar-Night dataset [49] and set depth range up to 60 meters. The best results are in **bold**.

|                              | Methods             | Abs Rel<br>lower's better | RMSE         | $\delta < 1.25$<br>higher's better |
|------------------------------|---------------------|---------------------------|--------------|------------------------------------|
| SOTA                         | Monodepth2          | 0.303                     | 5.045        | 0.458                              |
|                              | SRNSD [6]           | 0.169                     | 6.439        | 0.768                              |
|                              | md4All-AD           | 0.123                     | 3.812        | 0.857                              |
|                              | md4All-DD           | 0.123                     | 3.664        | 0.848                              |
| Plugin<br>Enhanced<br>Models | PhysDepth+DepthDark | 0.122                     | 3.666        | 0.875                              |
|                              | PhysDepth+ConvNeXt  | 0.122                     | 3.665        | 0.876                              |
|                              | PhysDepth+S2R       | 0.123                     | 3.662        | 0.879                              |
|                              | PhysDepth+ViT-B/16  | 0.121                     | 3.663        | 0.878                              |
| Ours                         | <b>PhysDepth</b>    | <b>0.120</b>              | <b>3.659</b> | <b>0.881</b>                       |

Table 15. **Ablation Study:** PhysDepth and Plugin-enhanced Models on all images from the RobotCar-Night dataset [49] and set depth range up to 80 meters. The best results are in **bold**.

|                              | Methods             | Abs Rel<br>lower's better | RMSE         | $\delta < 1.25$<br>higher's better |
|------------------------------|---------------------|---------------------------|--------------|------------------------------------|
| SOTA                         | Monodepth2          | 0.399                     | 6.641        | 0.744                              |
|                              | md4All-AD           | 0.124                     | 3.880        | 0.857                              |
|                              | md4All-DD           | 0.123                     | 3.713        | 0.849                              |
| Plugin<br>Enhanced<br>Models | PhysDepth+DepthDark | <b>0.121</b>              | 3.659        | 0.877                              |
|                              | PhysDepth+ConvNeXt  | <b>0.121</b>              | 3.662        | 0.874                              |
|                              | PhysDepth+S2R       | <b>0.121</b>              | 3.659        | 0.876                              |
|                              | PhysDepth+ViT-B/16  | <b>0.121</b>              | 3.658        | 0.877                              |
| Ours                         | <b>PhysDepth</b>    | <b>0.121</b>              | <b>3.657</b> | <b>0.879</b>                       |

ter the  $\beta$  value from 80 meters to 40, 50, and 60 meters, respectively.

The results show that PhysDepth outperforms SOTA methods in all distances, demonstrating PhysDepth’s robustness under challenging environments. Additionally, the plugin (PPM + Loss Functions) effectively enhanced existing MDE models.

Table 13, 14, and 15 show the results of RobotCar-Night dataset [27] with depth scales of 40, 60, and 80 meters, respectively. The results affirm that *PhysDepth can accurately estimate the depth under challenging environments despite the varying depth scales*. Notably, in Table 13, we significantly outperform Monodepth2 in RMSE.

### 11.2. Additional Ablation Study

Table 16. **Ablation Study of  $f(R)$  and  $R$ :** Using red channel images from the RobotCar-Night dataset [49] and the depth range is up to 80m. The best results are in **bold**.

| Methods           | Abs Rel<br>lower's better | RMSE         | $\delta < 1.25$<br>higher's better |
|-------------------|---------------------------|--------------|------------------------------------|
| PhysDepth+ $R$    | 0.147                     | 3.981        | 0.635                              |
| PhysDepth+ $f(R)$ | <b>0.121</b>              | <b>3.657</b> | <b>0.879</b>                       |

In Table 16, we use Equation 4 and Equation 6 to estimate  $d_R$  respectively.

PhysDepth +  $R$  shows the result from Equation 4. And PhysDepth +  $f(R)$  shows the result from Equation 6. These

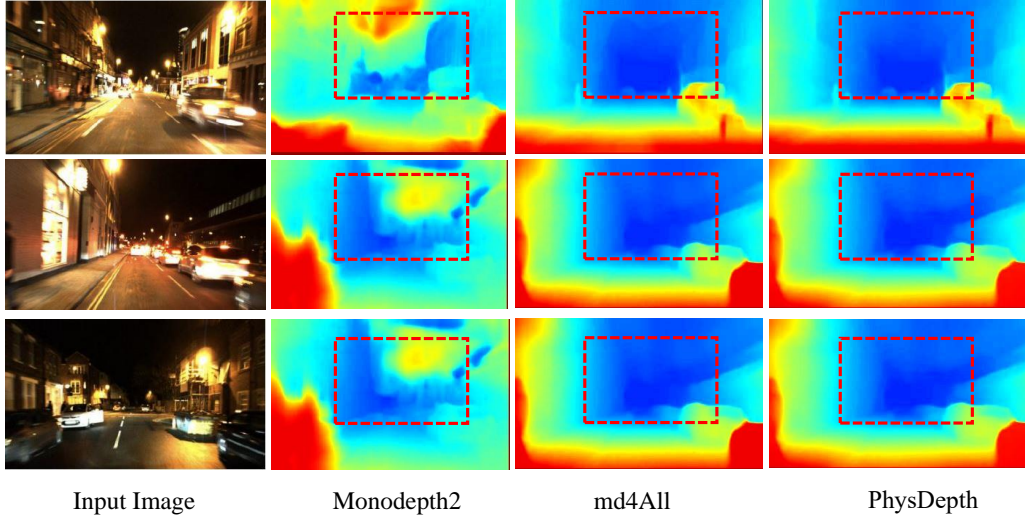


Figure 6. **Qualitative Results - RobotCar-Night:** Depth estimated on three different test images (column: Input Image) using our approach (column: PhysDepth) in comparison with two other methods (remaining columns).

results further demonstrating using  $f(R)$  is better than  $R$  in our model because  $f(R)$  contains low and high level feature from image.

$$I = I_0 \frac{1}{a \times d_R + b} \quad (8)$$

$$I = I_0 \frac{1}{a \times d_R^2 + b \times d_R + c} \quad (9)$$

Table 17. **Ablation Study of  $\mu$ :** Using different  $\mu$  on RobotCar-Night dataset [49] and the depth range is up to 80m. The best results are in **bold**.

| Methods                           | Abs Rel<br>lower's better | RMSE         | $\delta < 1.25$<br>higher's better |
|-----------------------------------|---------------------------|--------------|------------------------------------|
| $\mu=0.1$                         | 0.139                     | 4.875        | 0.315                              |
| $\mu=0.05$                        | 0.125                     | 4.362        | 0.741                              |
| $\mu=0.025$                       | 0.120                     | 4.257        | 0.853                              |
| <b>Learnable <math>\mu</math></b> | <b>0.121</b>              | <b>3.657</b> | <b>0.879</b>                       |

Table 17 presents the ablation study with different strategies to choose  $\mu$  in Equation 3; For the first strategy, we set  $\mu$  to a fixed value. To ensure a fair comparison, we respectively set  $\mu$  to 0.05, 0.025, and 0.0125, which are selected based on 80 meters' depth range. For the second strategy, we set  $\mu$  as a learnable parameter, which is the implementation of PhysDepth.

According to Table 17 and 18, setting  $\mu$  and  $\lambda$  as learnable parameters gives the best accuracy. This is because each pixel of the same input image may represent a unique light attenuation condition; dynamically assigning distinct

Table 18. **Ablation Study of  $\lambda$ :** Using different  $\lambda$  on RobotCar-Night dataset [49] and the depth range is up to 80m. The best results are in **bold**.

| Methods                               | Abs Rel<br>lower's better | RMSE         | $\delta < 1.25$<br>higher's better |
|---------------------------------------|---------------------------|--------------|------------------------------------|
| $\lambda=0.01$                        | 0.358                     | 9.182        | 0.980                              |
| $\lambda=0.1$                         | 0.227                     | 4.775        | 0.677                              |
| $\lambda=0.003$                       | 0.195                     | 3.951        | 0.451                              |
| <b>Learnable <math>\lambda</math></b> | <b>0.121</b>              | <b>3.657</b> | <b>0.879</b>                       |

$\mu$  and  $\lambda$  values to each pixel enables each pixel to automatically adjust to its own light attenuation conditions.

To determine the optimal value for the parameter  $g$  in Equation 5, we conducted empirical tests using various values. Our results, presented in Table 19, indicate that setting  $g$  to 1.3938 yields the highest accuracy.

We also test PhysDepth with multiple views (3, and 5 views) as input. However, the results exhibit negligible improvements, aligning with the conclusions of Ummenhofer et al. [44] and Zhou et al. [62].

## 12. Additional Qualitative Results

Figure 6 shows the results on the RobotCar-Night dataset, demonstrating that our model provides more accurate MDE results compared to others. For instance, The red boxes in Figure 6 - a,b,c

demonstrate our model's ability to accurately handle varying lighting conditions.

In Figures 7, we use nuScence-Night dataset to compare PhysDepth with SOTA methods: Monodepth2 [15] and

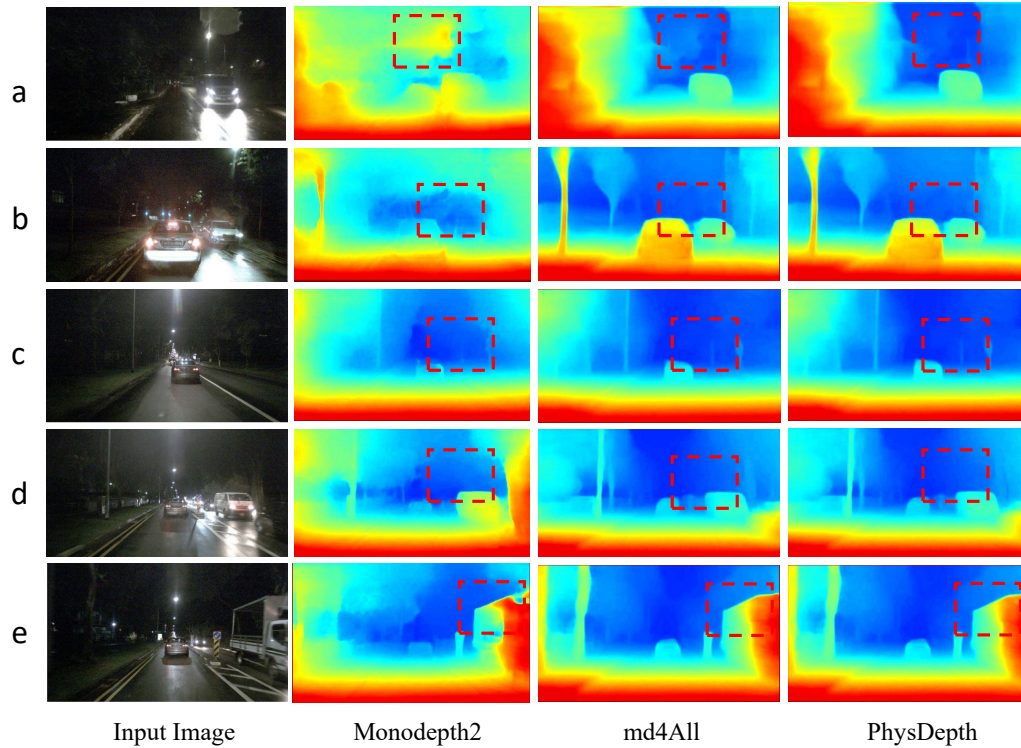


Figure 7. **Qualitative Results - nuScence-Night:** Depth estimated on five different test images (column: Input) using our approach (column: PhysDepth) in comparison with two SOTA methods (remaining columns).

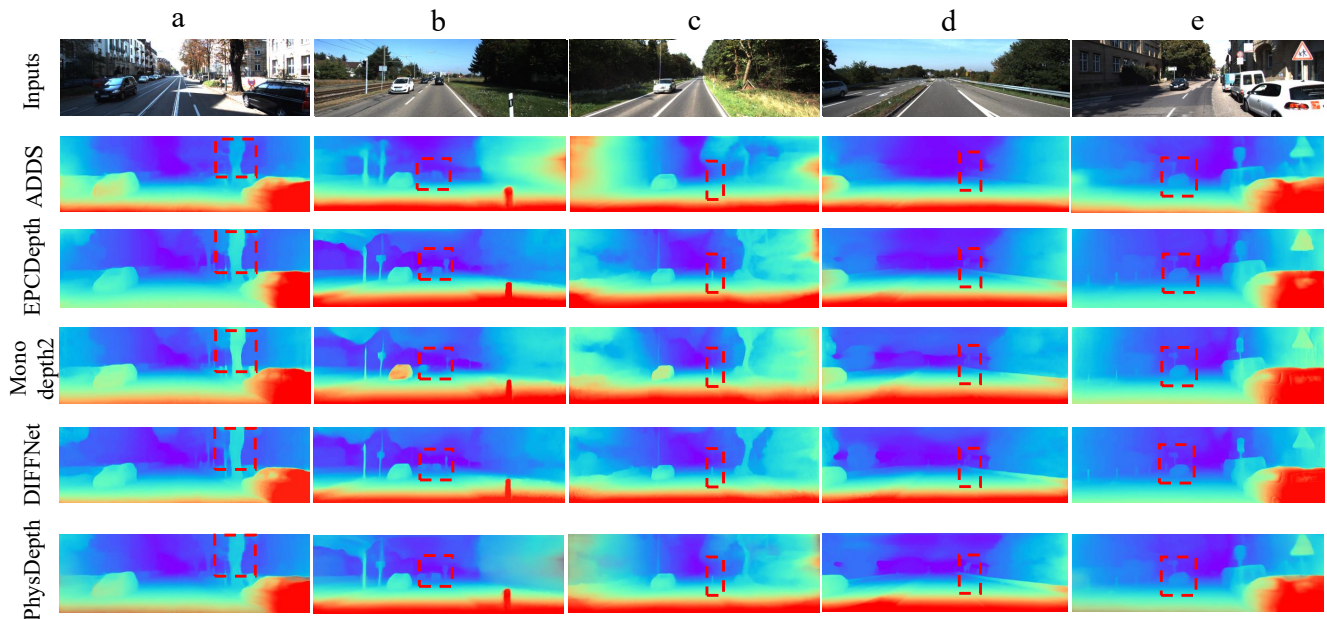


Figure 8. **Qualitative Results - KITTI:** Depth estimated on five different test images (row: Inputs) using our model (row: PhysDepth) and four SOTA (remaining rows) for comparison.

md4All [12]. From the results, PhysDepth shows sharper details for the roads and cars, showcasing PhysDepth’s abil-

ity to accurately handle varying light conditions under challenging scenarios.

Table 19. **Ablation Study of gg**: Using different gg on RobotCar-Night dataset [49] and the depth range is up to 80m. The best results are in **bold**.

| Methods    | Abs Rel      | RMSE         | $\delta < 1.25$<br>lower's better<br>higher's better |
|------------|--------------|--------------|--|
| $g=0.5$    | 0.921        | 6.175        | 0.710  |
| $g=0.1$    | 0.550        | 5.587        | 0.515  |
| $g=0.01$   | 0.515        | 5.251        | 0.355  |
| $g=1.5$    | 0.873        | 5.891        | 0.689  |
| $g=1.3938$ | <b>0.121</b> | <b>3.657</b> | <b>0.879</b>   |

Table 20. **Quantitative Results - KITTI [13]**: Comparison of our model on the KITTI test split by Eigen [8]. M means monocular image, and S means stereo image. The best results are in **bold** for each metric. All results presented here are without post-processing.

| Methods           | Data | $H \times W$ | Abs Rel        | RMSE            | $\delta < 1.25$ |
|-------------------|------|--------------|----------------|-----------------|-----------------|
|                   |      |              | lower's better | higher's better | higher's better |
| DynaDepth [10]    | S    | 192 × 640    | 0.109          | 4.705           | 0.869           |
| MonoDepth2 [15]   | S    | 320 × 1024   | 0.107          | 4.764           | 0.874           |
| EPCDepth [34]     | S    | 320 × 1024   | 0.091          | 4.207           | 0.901           |
| DepthFormer [23]  | S    | 320 × 1024   | 0.090          | 4.149           | 0.905           |
| PlaneDepth [50]   | S    | 384 × 1280   | 0.083          | 3.919           | 0.913           |
| <b>PhysDepth</b>  | S    | 320 × 1024   | <b>0.079</b>   | <b>3.915</b>    | <b>0.917</b>    |
| SfMLearner [62]   | M    | 128 × 416    | 0.198          | 6.565           | 0.718           |
| DeFeat-Net [41]   | M    | 352 × 480    | 0.126          | 5.035           | 0.862           |
| CADDepth-Net [53] | M    | 192 × 640    | 0.105          | 4.535           | 0.892           |
| FM [40]           | M    | 192 × 640    | 0.104          | 4.481           | 0.893           |
| GCP-MonoViT [28]  | M    | 192 × 640    | 0.096          | 4.327           | 0.904           |
| <b>PhysDepth</b>  | M    | 192 × 640    | <b>0.093</b>   | <b>4.013</b>    | <b>0.906</b>    |
| MonoDepth2 [15]   | M    | 320 × 1024   | 0.115          | 4.701           | 0.879           |
| DynamicDepth[10]  | M    | 192 × 640    | 0.103          | 5.867           | 0.897           |
| CADDepth-Net [53] | M    | 320 × 1024   | 0.102          | 4.407           | 0.898           |
| DIFFNet [32]      | M    | 320 × 1024   | 0.097          | 4.345           | 0.907           |
| <b>PhysDepth</b>  | M    | 320 × 1024   | <b>0.095</b>   | <b>3.995</b>    | <b>0.912</b>    |

Notably, the input images are particularly challenging as they were taken in extremely dark environments. However, PhysDepth can still provide robust results under those extreme conditions.

### 13. Evaluation on Daytime Dataset

We use KITTI [13] dataset to verify the performance of PhysDepth under daytime environments. Table 20 highlights that our model outperforms all SOTA models across all metrics, emphasizing its overall generality and accuracy under daytime environments.

Figure 8 qualitatively demonstrates that PhysDepth, while designed for MDE under challenging conditions, outperforms SOTA models under daytime scenarios. For example, in Figure 8 - b, our model accurately detects the car, providing clear and sharp boundaries. In contrast, MonoDepth2 fails to detect the car entirely. While ADDS, EPCDepth, and DIFFNet can locate the car, the boundaries they produce are noticeably blurred, resulting in the two cars being jammed together on the estimated depth maps. *The physical priors employed by PhysDepth are environment-invariant, ensuring robust performance in*

*both daytime scenarios and in challenging conditions..*

### 14. Failure Cases

PhysDepth performs well under challenging environments, but there's room for improvement with specific corner cases. For example, Figure 9 shows two instances of the failure cases.

In the input images, halos originating from road lamps and other car headlights are the main reasons for these failure cases. These halos give rise to shadows and reflections, which could affect the light attenuation item (Equation 3) in RCA loss, leading to compromised depth estimation results.

The halo issue is commonly known as one of the most challenging conditions in nighttime depth estimation [49]. From Figure 9, we can see that SOTA method md4All [12] produces similar depth results as PhysDepth, demonstrating that SOTA methods may not be able to handle the failure case well.

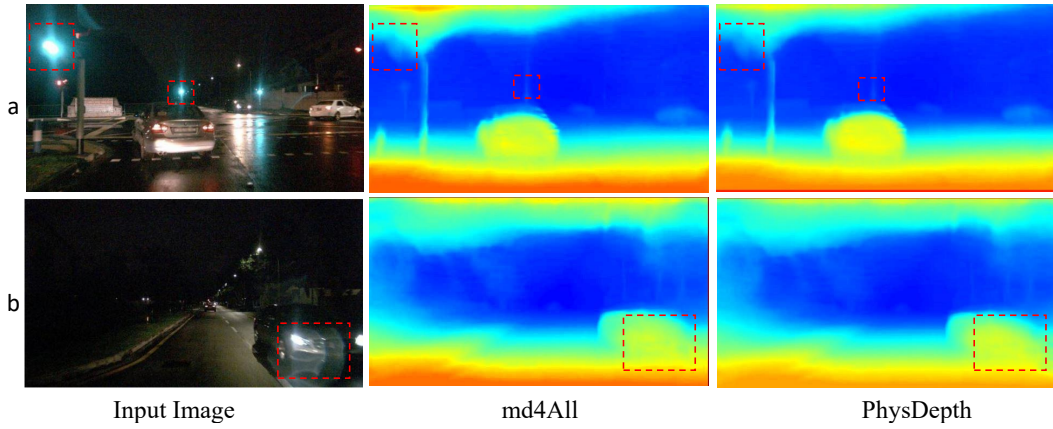


Figure 9. **Failure Cases - nuScence-Night:** Comparison between PhysDepth and md4All [12]. Red boxes show the halos because of road lamps and car headlights in the input image, which may cause failure for both PhysDepth and md4All.